Computers and Fluids 170 (2018) 299–312

Contents lists available at ScienceDirect

Computers and Fluids

journal homepage: www.elsevier.com/locate/compfluid

A combined compact finite difference scheme for predicting the evolution of a mean curvature driven interface

H.L. Wen [a], Tony W.H. Sheu [a,b,c,*], C.H. Yu [d]

[a] Department of Engineering Science and Ocean Engineering, National Taiwan University, No. 1, Sec. 4, Roosevelt Road, Taipei, Taiwan, Republic of China
[b] Institute of Applied Mathematical Sciences, National Taiwan University, PR China
[c] Center for Advanced Study in Theoretical Sciences, National Taiwan University, PR China
[d] State Key Laboratory of Hydraulics and Mountain River Engineering, Sichuan University, Sichuan 610000, PR China

ARTICLE INFO

Article history:
Received 6 October 2017
Revised 5 May 2018
Accepted 13 May 2018
Available online 15 May 2018

ABSTRACT

This study is aimed to develop a high-order finite difference scheme to simulate the mean curvature equation for accurately predicting the time-evolving mean curvature driven interface. Within the semi-discretization framework, the optimal third-order accurate temporal scheme is applied for the approximation of the time derivative term. In a three-point grid stencil, a combined compact difference scheme has been developed for offering a fifth-order spatial accuracy for the first-order and second-order derivative terms shown in the level set equation for simulating mean curvature flow. In the simulation of the mean curvature equation, reinitialization procedure has been performed to improve the prediction of curve motion. The aim of this study is to give insights into the issue about "how a mean curvature driven curve is varied with time". Two mechanisms leading to the change of curve slope are attributed partly to the damping Laplacian operator and partly to the embedded nonlinear differential operator. These mechanisms have been studied in detail with respect to the curvature of curve. The effect of performing reinitialization is also studied numerically.

1. Introduction

Study of geometric evolution of curves or surfaces has been an important subject in mathematical society. Research into this type of physical and mathematical problems has led to several systems of nonlinear partial differential equations. Many physical processes about the propagation of material interface, free surface or interface flow development, and the growth of crystal can be simulated by solving the corresponding partial differential equations governing the evolution of geometrical curves or surfaces. An accurate capturing of these time-evolving curves and surfaces is essential for gaining a better understanding of the convection and diffusion phenomena in many curve and surface processing applications. In computer graphics, the processing of triangulated surfaces, for example, is a fundamental topic worth of investigation as well [1].

In the mathematical modeling of a geometric evolution of curve or interface Γ, one can represent it implicitly as the zero level set of a continuous function ϕ. This corresponds to writing $\Gamma = \{\underline{x}|\phi(\underline{x},t)=0\}$ for a surface. In many problems ranging from a two-fluid flow to a crystal growth process, the evolution is subject to the normal speed of Γ. The time evolution of the level set function ϕ for this class of problems can be expressed in a general form as $\frac{\partial\phi}{\partial t}+u_N|\nabla\phi|=0$, where the normal speed of Γ differs from each other depending on their involved physical mechanisms leading to the change of ϕ. For the mean curvature flow problem, $u_N=-\kappa$, where κ $(\equiv\nabla\cdot\vec{n})$ is the mean curvature of Γ, $\nabla\cdot$ is the surface divergence differential operator, and $\vec{n}$ denotes the outward normal vector of the curve of interest. The level set equation for modeling the motion driven by mean curvature becomes

$$\frac{\partial\phi}{\partial t}-\nabla\cdot\left(\frac{\nabla\phi}{|\nabla\phi|}\right)|\nabla\phi|=0 \tag{1}$$

Surface diffusion occurring in film growth is the other example of the physical effect that is relevant to the evolution of geometric curves. For this case, surface Γ moves with the normal velocity $\nabla_s\cdot(\nabla_s\kappa)$ under surface diffusion, where $\nabla_s=\nabla-\hat{n}(\hat{n}\cdot\nabla)$. The change of the level set function ϕ for surface diffusion corresponds to

$$\frac{\partial\phi}{\partial t}+\nabla_s\cdot\nabla_s\kappa|\nabla\phi|=0 \tag{2}$$

* Corresponding author at: Department of Engineering Science and Ocean Engineering, National Taiwan University, No. 1, Sec. 4, Roosevelt Road, Taipei, Taiwan, Republic of China.
E-mail address: twhsheu@ntu.edu.tw (T.W.H. Sheu).

https://doi.org/10.1016/j.compfluid.2018.05.013
0045-7930/

Due to the similarity presenting in two important classes of equation, it is worthwhile for us to investigate the equation generalized as $\frac{\partial \phi}{\partial t} + u_N|\nabla\phi| = 0$, where $u_N = -\nabla \cdot (\frac{\nabla\phi}{|\nabla\phi|})$ for mean curvature flow while $u_N = \nabla_s \cdot (\nabla_s \kappa)$ for surface diffusion flow. In our study employing the level set method, the focus will be on the evolution of geometric curve driven by its mean curvature. Motions of curves subject to surface diffusion have been predicted by different research groups [7–9] using the level set method.

The content of this paper will be organized as follows. In Section 2, the level set equation for the modeling of a time-evolving curve driven by mean curvature and surface diffusion will be presented. Some important features of this equation cast in level set function will be pointed out. The numerical method will be introduced in Section 3. In Section 4, the nonlinear parabolic equation will be solved using the high-order compact finite difference scheme formulated in a three-point grid stencil. Discussion of the simulated results will be given in Section 4 as well. Finally, we will draw some concluding remarks in Section 5.

2. Level set equation

In real life, diffusion process, which is well-known as $\frac{\partial c}{\partial t} = D\nabla^2 c$, equilibrates spatial change of a physical concentration c. Such a process involving the molecular diffusion coefficient D happens all the time and is irreversible. For the evolution of a smoothly distributed surface $\underline{x}$, the Eulerian Laplacian differential operator ∇^2 is replaced with the Laplace Beltrami differential ∇_M, leading to the so-called geometric diffusion analogue for the coordinate $\underline{x}$ on a surface S.

$$\frac{\partial \underline{x}}{\partial t} = \nabla_M^2(t)\underline{x} \tag{3}$$

According to the theory of differential geometry [2], the Laplace Beltrami operator defined on a surface S is identical to the mean-curvature vector $h(\underline{x})n(\underline{x})$, implying that

$$-\nabla_M^2 \underline{x} = h(\underline{x})\ n(\underline{x}) \tag{4}$$

Geometric diffusion is commonly referred to as mean curvature motion, thereby leading to the following differential equation

$$\frac{\partial \underline{x}}{\partial t} = -h(\underline{x})\ n(\underline{x}) \tag{5}$$

In the above, $h(\underline{x})$ denotes the mean curvature and $n(\underline{x})$ can be expressed in terms of the level set function ϕ as

$$n(\underline{x}) = |\nabla\phi| \tag{6}$$

The mean curvature, which is defined as the sum of the two principal curvatures, can be written as $\nabla \cdot \vec{n} = \nabla \cdot (\frac{\nabla\phi}{|\nabla\phi|})$, where the distance function is negative inside the curve. In two-dimensional domain, the curvature of a curve can be explicitly expressed as

$$h(\underline{x}) = \nabla \cdot (\frac{\nabla\phi}{|\nabla\phi|}) = \frac{\phi_{xx}\phi_y^2 - 2\phi_x\phi_y + \phi_{yy}\phi_x^2}{(\phi_x^2 + \phi_y^2)^{3/2}} \tag{7}$$

Given the definitions of $n(\underline{x})$ and $h(\underline{x})$, the partial differential equation for geometric diffusion can be derived in terms of a level set function as

$$\frac{\partial \phi}{\partial t} - |\nabla\phi|\ \nabla \cdot (\frac{\nabla\phi}{|\nabla\phi|}) = 0 \tag{8}$$

In this study, we aim to investigate the Cauchy problem that involves the Hamiltonian–Jacobi Eq. (8) cast in the first order form. Eq. (8) can be also expressed differently as follows after a mathematical manipulation.

$$\frac{\partial \phi}{\partial t} = \nabla^2\phi - N(\phi) \tag{9}$$

where

$$N(\phi) = \frac{\partial|\nabla\phi|}{\partial n} = \frac{\nabla\phi}{|\nabla\phi|} \cdot \nabla(|\nabla\phi|) \tag{10}$$

Eq. (9) elucidates that surface diffusion has a role to play in the mean curvature flow equation.

The level set method, developed by Osher and Sethian [4], will be applied to predict the motion of interface in a domain of two dimensions. Level set methods have been applied with great success to predict a wide variety of problems. One can refer to the review papers [5–7]. For the level set function ϕ in a flow field $\underline{u}$, it is mathematically modeled by the well-known pure advection equation.

$$\frac{\partial \phi}{\partial t} + \underline{u} \cdot \nabla\phi = 0 \tag{11}$$

If the evolution of curves or surfaces involves only the normal component of $\underline{u}$, we can get

$$\frac{\partial \phi}{\partial t} + u_n\ |\nabla\phi| = 0 \tag{12}$$

By comparing the Eq. (8) with the nonlinear parabolic Eq. (12), we are led to get the normal speed of the surface

$$u_n = -\nabla \cdot (\frac{\nabla\phi}{|\nabla\phi|}) \tag{13}$$

As we mentioned in the introduction, it is worthy to point out the similarity and difference between the mean curvature flow and the surface diffusion flow. By virtue of the classification of these two equations, both of them are parabolic equations but they are driven by different normal speeds related to the curvature. Eq. (13) shows that the normal speed of mean curvature flow is the mean curvature. As for Eq. (2), the normal speed of surface diffusion flow is

$$u_n = \nabla_s^2\kappa = \nabla^2\kappa - (\vec{n} \cdot \nabla)(\vec{n} \cdot \nabla\kappa) \tag{14}$$

The physical meaning of the term on the right-hand-side of Eq. (14) is that the normal speed of curve in surface diffusion flow depends only on the physical diffusion of curvature along the curves. The first term on the right-hand-side denotes the diffusion of curvature over the space, and the second term stands for the diffusion on its normal direction of the curve. The result enlightens the presence of the tangential diffusion of curvature along the curves. It is worthy to note here that the difficulty of solving Eq. (12) with respect to two different types of curve motion subjected to different normal speeds, as shown in Eqs. (13) and (14), for an interface motion is that it is nonlinear and is quite stiff. We are therefore motivated to propose a numerically very accurate and computationally more efficient method.

3. Numerical method

The primary difficulty of numerically solving the level set equation for a motion driven by mean curvature is that the parabolic Eq. (12) is stiff. Implicit method is therefore the method of choice for the finite difference approximation of the Hamiltonian–Jacobi equation for the modeling of curvature flow motion [3]. Moreover, Eq. (12) is nonlinear. It is therefore a straightforward practice for us to implement implicit numerical method in this study to circumvent the computational difficulty.

In this paper, we rewrite Eq. (12) in the form of

$$\phi_t = L(\phi) \tag{15}$$

where

$$L(\phi) = -u_n|\nabla\phi| \tag{16}$$

The solution to the parabolic Eq. (15) will be sought subject to the initial condition given by

$$\phi(\underline{x}, t=0) = \phi_0 \tag{17}$$

The semi-discretization scheme will be employed to solve the Eq. (15). The time discretization is performed first using the Runge–Kutta method with the initial condition (17) and, then, the spatial discretization will be performed.

3.1. Optimal third-order TVD Runge–Kutta temporal scheme

The Runge–Kutta method for Eq. (15) can be expressed in a general form as follows for $i = 1, \ldots, m$ [10].

$$\phi^{(i)} = \sum_{k=0}^{i-1} \alpha_{ik}\, \phi^{(k)} + \Delta t\, \beta_{ik}\, L(\phi^{(k)}) \tag{18}$$

$$\phi^0 = \phi^n, \phi^m = \phi^{n+1} \tag{19}$$

In the above class of Runge–Kutta schemes, the coefficients α_{ik} and β_{ik} shall be properly chosen so that application of the resulting scheme can not only yield higher order accuracy but also can maintain numerical stability in whatever the norms are [11]. We are therefore motivated to adopt a high order TVD (total variation diminishing) time discretization scheme [11]. Application of this class of schemes implies that the total variation of the numerical solution is not allowed to increase in the sense that $TV(\phi^{n+1}) \leq TV(\phi^n)$, where $TV(\phi) = \sum_i |\phi_{i+1} - \phi_i|$. Eq. (18) is TVD provided that α_{ik}, $\beta_{ik} \geq 0$ under a suitable time step restriction.

Our objective of employing the TVD Runge–Kutta scheme is to retain the TVD property while high order temporal accuracy can be maintained. To achieve the goal of obtaining high-order solution accuracy and enhancing numerical stability, it is required that both coefficients α_{ik} and β_{ik} shown in Eq. (18) be non-negative. Therefore, the optimal third-order TVD Runge–Kutta method given in [11] is adopted.

$$\begin{aligned}
\phi^1 &= \phi^n + \Delta t\, L(\phi^n) \\
\phi^2 &= \frac{3}{4}\phi^n + \frac{1}{4}\phi^1 + \frac{1}{4}\Delta t\, L(\phi^1) \\
\phi^{n+1} &= \frac{1}{3}\phi^n + \frac{2}{3}\phi^2 + \frac{2}{3}\Delta t\, L(\phi^2)
\end{aligned} \tag{20}$$

The above scheme is stable subject to the CFL condition, by which we have

$$c = \frac{\Delta t}{\Delta x} \leq \min_{i,k}\left(\frac{\alpha_{ik}}{\beta_{ik}}\right)$$

3.2. Combined compact finite difference scheme for spatial derivative terms

Having discretized the temporal derivative term in Eq. (20), we proceed to the discretization of the spatial derivative terms $L(\phi^n), L(\phi^1)$ and $L(\phi^2)$ shown in Eq. (20). The idea of applying the combined compact difference (CCD) scheme proposed first by Chu and Fan [12] is to improve prediction accuracy when approximating the first and second order derivative terms without increasing the number of stencil points. The building block of our CCD scheme is to calculate the derivative of a function at an interior grid point together with the same derivative terms at the two adjacent points. With the ability of improving solution accuracy with lower computational cost, it is quite promising that CCD scheme can be implemented for large scale computation.

In Eq. (7), one can see clearly that calculation of the curvature of a curve Γ involves computing the values of ϕ_x, ϕ_y, ϕ_{xx}, ϕ_{yy} and ϕ_{xy}. To get a spectral-like resolution for these derivatives in a grid involving only three stencil points, $i-1, i, i+1$, the centered CCD scheme is adopted in a domain with uniform spacing $h = \Delta x = \Delta y$. This CCD scheme calculates the derivative terms ϕ_x and ϕ_{xx} shown in (7) implicitly from the following two equations for $P \equiv \phi_x$ and $Q \equiv \phi_{xx}$.

$$\begin{aligned}
&\frac{7}{16}(P_{i+1} + P_{i-1}) + P_i - \frac{h}{16}(Q_{i+1} - Q_{i-1}) = \frac{15}{16h}(\phi_{i+1} - \phi_{i-1}) \\
&\frac{9}{8h}(P_{i+1} - P_{i-1}) - \frac{1}{8}(Q_{i+1} + Q_{i-1}) + Q_i = \frac{3}{h^2}(\phi_{i+1} - 2\phi_i + \phi_{i-1})
\end{aligned} \tag{21}$$

All the coefficients shown in (21) have been derived underlying the modified equation analysis. Taylor series expansion has been performed on P_{i+1} and Q_{i+1} with respect to P_i and Q_i, respectively, to get the corresponding modified equations. The leading error terms in the modified equations are then eliminated to close the derivation of the two equations in (21). Similar idea can be employed to implicitly calculate the nodal values of ϕ_y and ϕ_{yy} by solving the resulting block tri-diagonal matrix. As for the value of ϕ_{xy}, it can be also computed by taking this mixed derivative term as the differentiation of ϕ_y with respect to x.

3.3. Distance reinitialization

In the prediction of geometric evolution of a curve Γ, one should prevent the level set function ϕ becoming too flat or too steep near Γ that separates two fluids [4]. Avoidance of this issue that has been known to arise more or less from the introduced discretization error necessitates the application of a distance reinitialization procedure. The level set function ϕ governed by Eq. (8) should be replaced with the other signed distance function $d(\underline{x}, t)$, which denotes the signed distance of $\underline{x}$ to the closest point on Γ. By definition, the signed distance function is differentiable almost everywhere, and its gradient should satisfy the eikonal function $|\nabla\phi| = 1$ in the domain of interest. According to [13], the value of $\phi(\underline{x}, t)$ governed by (12) is reinitialized to the steady solution of the following equation for $\psi(\underline{x}, t)$, subject to $\psi(\underline{x}, \tau = 0) = \phi(\underline{x}, t) = \psi_0$,

$$\frac{\partial\psi}{\partial\tau} + sgn(\psi_0)\,(|\nabla\psi| - 1) = 0 \tag{22}$$

In the above, τ denotes the artificial time and $sgn(\psi) = 2H(\psi) - 1$, where $H(\psi)$ is known as the Heaviside function. Solution to Eq. (22) is sought with the time step of $\Delta\tau = 0.25\ \Delta x$. In other words, as $\tau \to \infty$, the solution ψ to Eq. (22) satisfies the eikonal function $|\nabla\psi| = 1$, and the reinitialization procedure is completed. The Heaviside function is the characteristic function, which is defined as

$$H(\psi) = \begin{cases} 0, & \text{if } \psi < \epsilon \\ \frac{1}{2}\left(1 + \frac{\psi}{\epsilon} + \frac{1}{\pi}\sin\left(\frac{\pi\psi}{\epsilon}\right)\right), & \text{if } |\psi| \leq \epsilon \\ 1, & \text{if } \psi > \epsilon \end{cases}$$

It is noted thatϵ is a small positive number with the value of $\epsilon = 1.5\ \Delta x$ in this study. Such a chosen magnitude can give us a better convergent result [16]. Eq. (22) governing the evolution of distance function $\psi(\underline{x}, t)$ involves using the Heaviside function in the physical domain Ω. To avoid oscillatory solutions generated in the vicinity of Γ, we apply the WENO (Weighted Essential Non-Oscillatory) spatial discretization scheme [14,15] to get a high-resolution solution. In our employed closest point formulation of the distance function, the sign function $sgn(\phi)$ is approximated by introducing a small positive parameter ϵ to replace Eq. (22) with the following smoothed redistancing embedding partial differential equation.

$$\frac{\partial\psi}{\partial\tau} + \big(2H(\psi_0) - 1\big)(|\nabla\psi| - 1) = 0 \tag{23}$$

In the above, the sign function has been replaced with a smoother version. Eq. (23) can be also written into the following Hamiltonian–Jacobi form:

$$\psi_\tau + sgn(\psi_0)H(\psi, \nabla\psi) = 0 \tag{24}$$

where $H(\phi, \nabla\phi)$ is the corresponding Hamiltonian. By employing Godunov spatial discretization, Eq. (24) can be further rewritten in terms of the one-sided derivatives $\psi_x^+, \psi_x^-, \psi_y^+, \psi_y^-$ as

$$\psi_\tau + sgn(\phi_0)H^G(\psi_x^+, \psi_x^-, \psi_y^+, \psi_y^-) = 0 \tag{25}$$

In the above equation, H^G is function of one-sided derivatives.

$$H^G(\psi_x^+, \psi_x^-, \psi_y^+, \psi_y^-) = \begin{cases} \text{if } sgn(\phi) \le 0, \\ \sqrt{\max\left[((\psi_x^+)^p)^2, ((\psi_x^-)^m)^2\right] + \max\left[((\psi_y^+)^p)^2, ((\psi_y^-)^m)^2\right]} - 1 \\ \text{if } sgn(\phi) > 0, \\ \sqrt{\max\left[((\psi_x^+)^m)^2, ((\psi_x^-)^p)^2\right] + \max\left[((\psi_y^+)^m)^2, ((\psi_y^-)^p)^2\right]} - 1 \end{cases} \tag{26}$$

Noted that the notations $(\#)^p = \max(\#, 0)$ and $(\#)^m = \min(\#, 0)$. The one-sided derivatives $\psi_x^+, \psi_x^-, \psi_y^+, \psi_y^-$ are calculated as follows following the framework of WENO scheme. Consider a one-dimensional example, the definitions of ψ_x^+, ψ_x^- are respectively as follows

$$\left.\psi_x^+\right|_i = \frac{\hat{\psi}_{i+1/2}^+ - \hat{\psi}_{i-1/2}^+}{x_{i+1/2} - x_{i-1/2}}$$
$$\left.\psi_x^-\right|_i = \frac{\hat{\psi}_{i+1/2}^- - \hat{\psi}_{i-1/2}^-}{x_{i+1/2} - x_{i-1/2}} \tag{27}$$

The numerical fluxes of $\hat{\psi}_{i+1/2}^+, \hat{\psi}_{i+1/2}^-$ are the Lipschitz continuous functions of several neighboring values ψ_i. The numerical flux $\hat{\psi}_{i+1/2}^+, \hat{\psi}_{i+1/2}^-$ should be respectively computed within the WENO framework of the right and left biased interpolations. Construction of the right-biased and left-biased numerical fluxes is given as follows [15,17]

$$\hat{\psi}_{i+\frac{1}{2}}^- = \omega_1^L\hat{\psi}_{i+\frac{1}{2},L}^{(1)} + \omega_2^L\hat{\psi}_{i+\frac{1}{2},L}^{(2)} + \omega_3^L\hat{\psi}_{i+\frac{1}{2},L}^{(3)}$$
$$\hat{\psi}_{i+\frac{1}{2}}^+ = \omega_1^R\hat{\psi}_{i+\frac{1}{2},R}^{(1)} + \omega_2^R\hat{\psi}_{i+\frac{1}{2},R}^{(2)} + \omega_3^R\hat{\psi}_{i+\frac{1}{2},R}^{(3)} \tag{28}$$

In the above, $\hat{\psi}_{i+\frac{1}{2},R}^{(k)}$ and $\hat{\psi}_{i+\frac{1}{2},L}^{(k)}$ $(k = 1, 2, 3)$ are respectively expressed as

$$\hat{\psi}_{i+\frac{1}{2},L}^{(1)} = \frac{1}{3}\psi_{i-2} - \frac{7}{6}\psi_{i-1} + \frac{11}{6}\psi_i,$$
$$\hat{\psi}_{i+\frac{1}{2},R}^{(1)} = \frac{11}{6}\psi_{i+1} - \frac{7}{6}\psi_{i+2} + \frac{1}{3}\psi_{i+3}$$
$$\hat{\psi}_{i+\frac{1}{2},L}^{(2)} = -\frac{1}{6}\psi_{i-1} + \frac{5}{6}\psi_i + \frac{1}{3}\psi_{i+1}$$
$$\hat{\psi}_{i+\frac{1}{2},R}^{(2)} = \frac{1}{3}\psi_i + \frac{5}{6}\psi_{i+1} - \frac{1}{6}\psi_{i+2}$$
$$\hat{\psi}_{i+\frac{1}{2},L}^{(3)} = \frac{1}{3}\psi_i + \frac{5}{6}\psi_{i+1} - \frac{1}{6}\psi_{i+2}$$
$$\hat{\psi}_{i+\frac{1}{2},R}^{(3)} = -\frac{1}{6}\psi_{i-1} + \frac{5}{6}\psi_i + \frac{1}{3}\psi_{i+1} \tag{29}$$

The weighting coefficients $w_k^{R,L}$ $(k = 1, 2, 3)$ shown in (28) are nonlinear. This WENO scheme can make the linear differential Eq. (23) to become its nonlinear counterpart. As a result, non-oscillatory solution can be possibly obtained. The coefficients $w_k^{R,L}$ derived in [17] can yield the fifth-order accurate spatial discretization provided that

$$\omega_k^{R,L} = \frac{\alpha_k^{R,L}}{\sum_k \alpha_k^{R,L}},\ \alpha_k^{R,L} = \frac{c_k}{(\beta_k^{R,L} + \hat{\varepsilon})^2} \tag{30}$$

In the above, $\beta_k^{R,L}$ are the smoothness indicators of the kth stencil, and $\hat{\varepsilon}$ is a small positive number (10^{-12}) introduced to prevent division by zero. The smoothness indicators β_k $(k = 1, 2, 3)$ for the left-biased are shown as follows

$$\beta_1^L = \frac{13}{12}(\psi_{i-2} - 2\psi_{i-1} + \psi_i)^2 + \frac{1}{4}(\psi_{i-2} - 4\psi_{i-1} + 3\psi_i)^2$$
$$\beta_2^L = \frac{13}{12}(\psi_{i-1} - 2\psi_i + \psi_{i+1})^2 + \frac{1}{4}(\psi_{i-1} - \psi_{i+1})^2$$
$$\beta_3^L = \frac{13}{12}(\psi_i - 2\psi_{i+1} + \psi_{i+2})^2 + \frac{1}{4}(3\psi_i - 4\psi_{i+1} + \psi_{i+2})^2 \tag{31}$$

As for the smoothness indicators for the right-biased β_k $(k = 1, 2, 3)$, they are expressed as

$$\beta_1^R = \frac{13}{12}(\psi_{i+1} - 2\psi_{i+2} + \psi_{i+3})^2 + \frac{1}{4}(3\psi_{i+1} - 4\psi_{i+2} + \psi_{i+3})^2$$
$$\beta_2^R = \frac{13}{12}(\psi_i - 2\psi_{i+1} + \psi_{i+2})^2 + \frac{1}{4}(\psi_i - \psi_{i+2})^2$$
$$\beta_3^R = \frac{13}{12}(\psi_{i-1} - 2\psi_i + \psi_{i+1})^2 + \frac{1}{4}(\psi_{i-1} - 4\psi_i + 3\psi_{i+1})^2 \tag{32}$$

The optimal weights shown in (30) are $c_1 = 1/10$, $c_2 = 6/10$, $c_3 = 3/10$, which yield the fifth order accuracy in the approximation of the spatial derivative terms.

For clarification, the algorithm of the reinitialization procedure is summarized below:

- Beginning of the reinitialization procedure.
- Iteration starts –
- Calculate the smoothness indicators $\beta_k^{R,L}$ $(k = 1, 2, 3)$ from equations (31) and (32).
- Compute the corresponding nonlinear weighting coefficients $\omega_k^{R,L}$ $(k = 1, 2, 3)$ from Eq. (30).
- Calculate $\hat{\psi}_{i+1/2}^+$ and $\hat{\psi}_{i+1/2}^-$ with the nonlinear weighting coefficients from equations (28) and (29).
- Compute the one-sided derivatives from Eq. (27).
- Calculate H^G from Eq. (26).
- Update ψ by solving Eq. (25).
- Iteration stops until the solution reaches steady state condition –
- As reinitialization procedure is completed, let $\phi = \psi$

4. Numerical results

4.1. Order of reinitialization

To show the order of method we used in reinitialization, we investigated the problem introduced in [20] and [19]. The level set function is initialized with the following equation in a computational domain $\Omega : [-5, 5] \times [-5, 5]$.

$$\phi_0 = \left(0.1 + (x-3)^2 + (y-3)^2\right)\left(3 - \sqrt{x^2 + y^2}\right)$$

To evaluate the order of our method, the L_1 norm of the difference e_1 between the exact signed distance function and the numerical solution is determined by

$$e_1 = ||\phi^{exact} - \phi^{numerical}||_1 = \frac{1}{N_\Omega}\sum_\Omega \left|3 - \sqrt{x_{i,j}^2 + y_{i,j}^2} - \phi_{i,j}^{numerical}\right|$$

The corresponding L_1 norm errors e_1 obtained under different mesh sizes using different methods are listed in following table

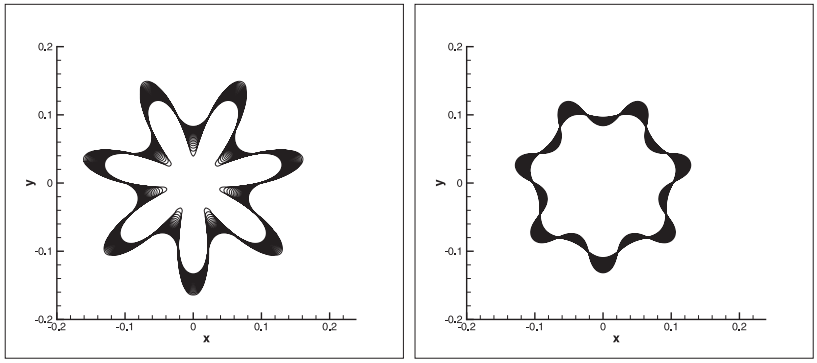

(a) $t = 0 - 0.0004$ (b) $t = 0.0004 - 0.0008$

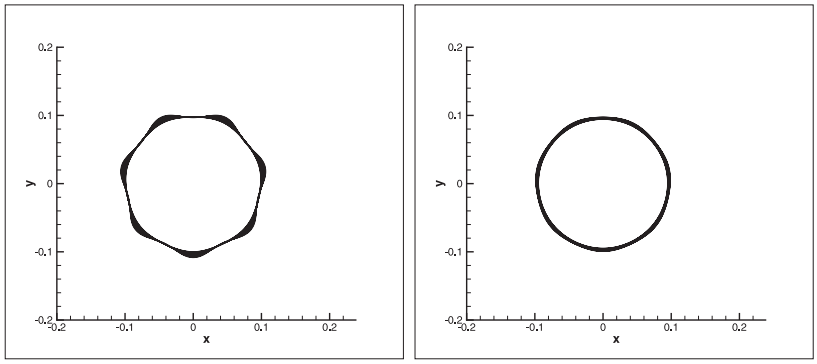

(c) $t = 0.0008 - 0.0012$ (d) $t = 0.0012 - 0.0016$

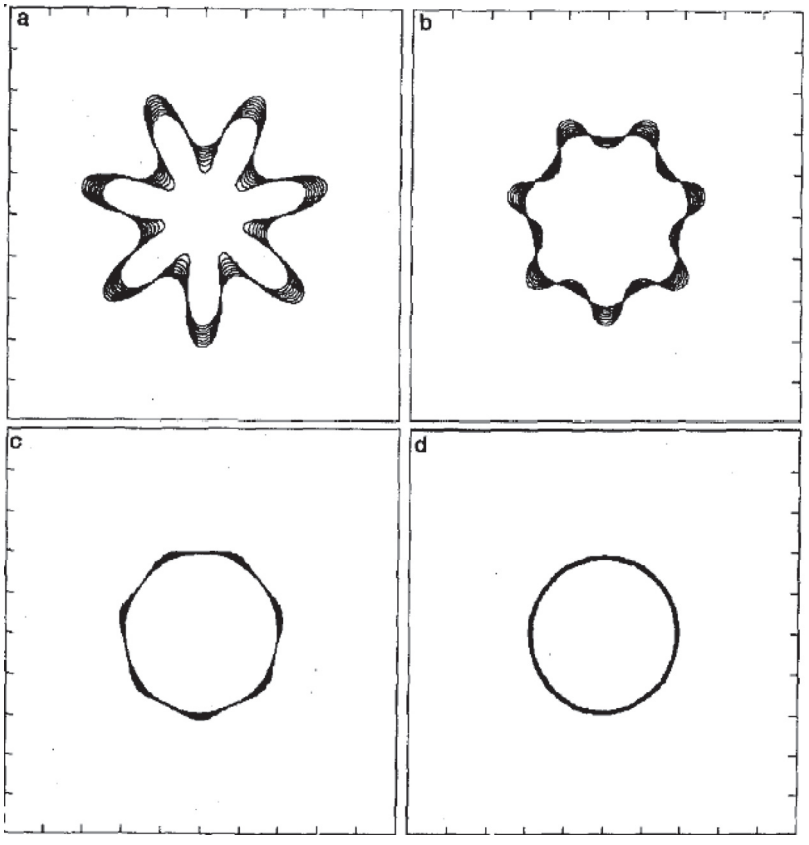

(e)

Fig. 1. Validation 1, present (a)–(d), ref. [18], (e) Star-shaped curve's motion by mean curvature. The computation is carried out in 300×300 grids, with the mesh size of $h = dx = dy$ and the time step of $dt = 0.0001 \times h$.

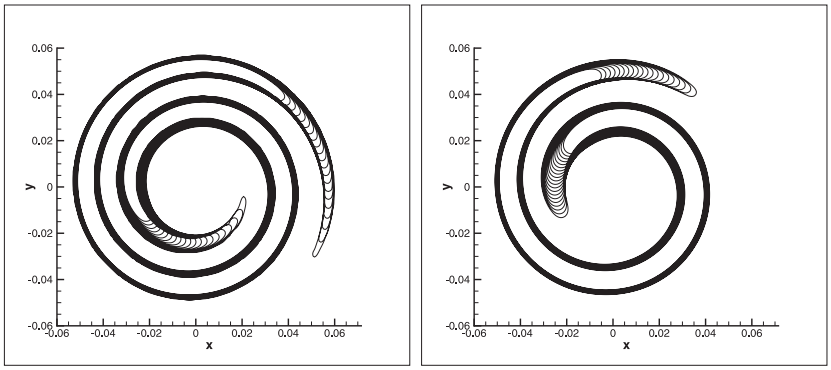

(a) $t = 0 - 0.0001$ (b) $t = 0.0001 - 0.0002$

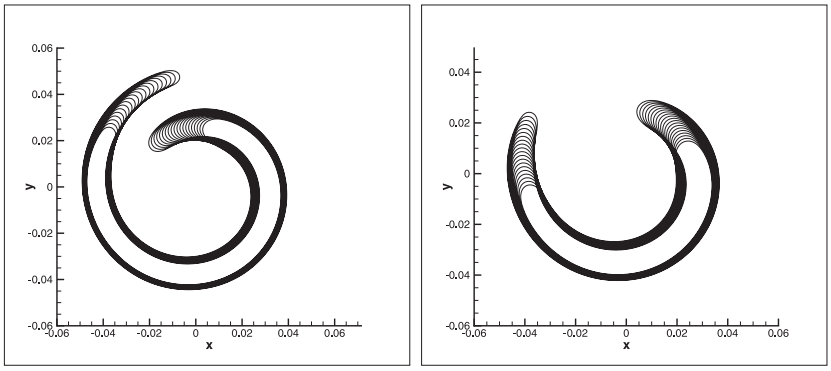

(c) $t = 0.0002 - 0.0003$ (d) $t = 0.0003 - 0.0004$

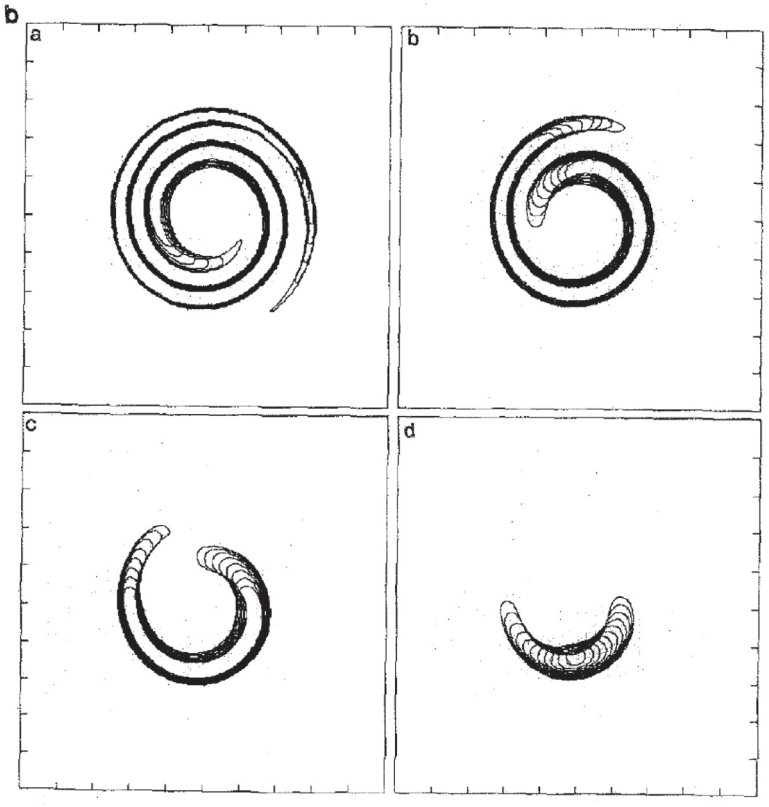

(e)

Fig. 2. Validation 2, present (a)–(d), ref. [18], (e) Wound spiral motion by mean curvature. The computation is carried out in 300×300 grids, with the mesh size of $h = dx = dy$ and the time step of $dt = 0.00001 \times h$.

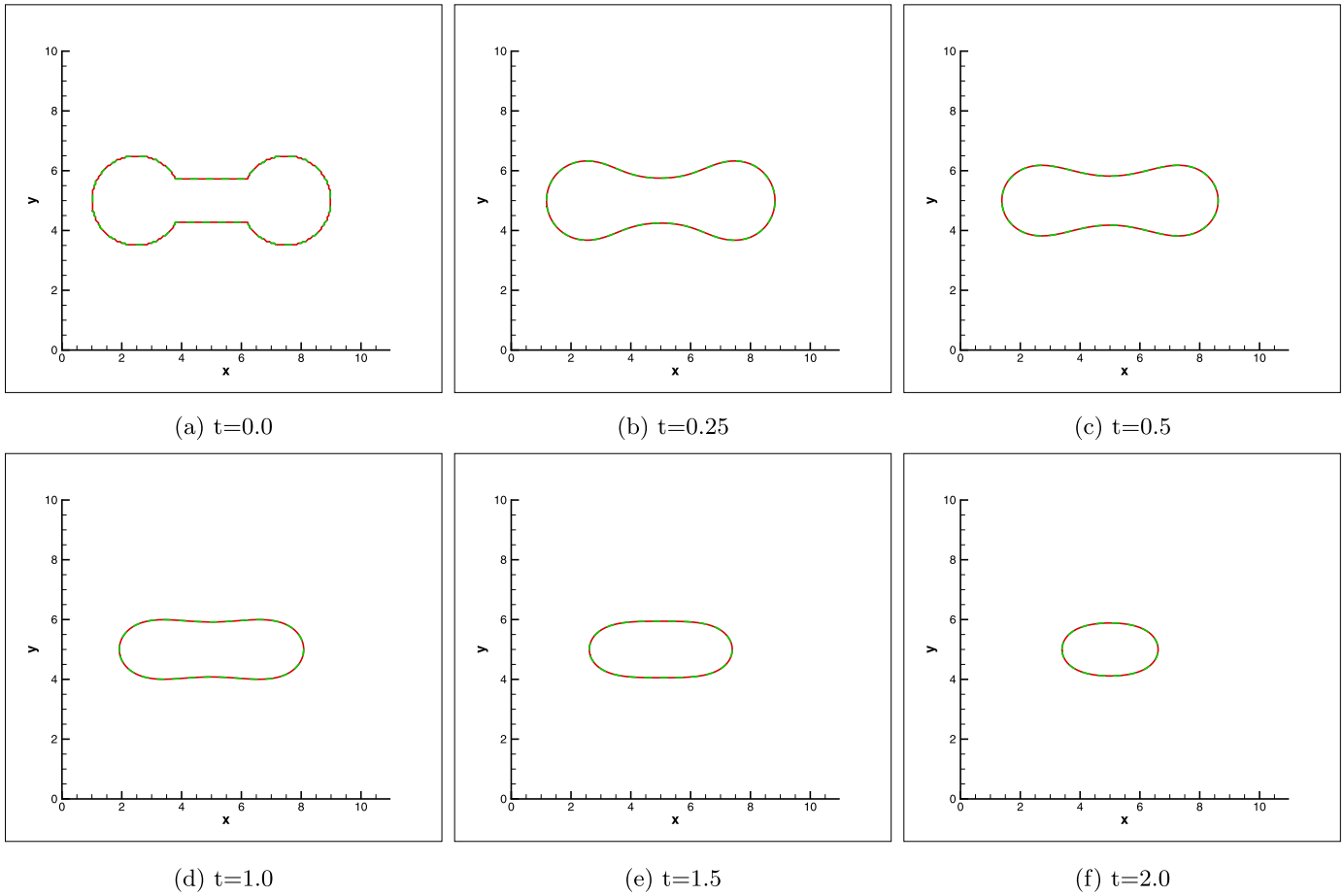

Fig. 3. Case 1. Computation is carried out in 200×200 grids in a 10 by 10 domain, with the mesh size of $h = \Delta x = \Delta y = 0.05$ and the time step of $\Delta t = 0.01 \times h$. Red line denotes the solution obtained with reinitialization procedure while green dashed line denotes the solution obtained without reinitializtion procedure. (For interpretation of the references to colour in this figure legend, the reader is referred to the web version of this article.)

Scheme	Mesh size	L_1 norm error	Order
Present method	10/64	3.419×10^{-4}	–
	10/128	3.109×10^{-5}	3.45
	10/256	3.833×10^{-6}	3.02
[19] (CR-1)	10/64	1.273×10^{-3}	–
	10/128	3.060×10^{-4}	2.1
	10/256	7.646×10^{-5}	2.0
[20] (RSC)	10/64	2.000×10^{-3}	–
	10/128	4.958×10^{-4}	2.0
	10/256	1.211×10^{-4}	2.0

4.2. Validation

Our validation studies were carried out by comparing the simulated results with the numerical result obtained by Osher and Sethian in [18]. Good agreement between two sets of the results can be clearly seen in Figs. 1 and 2 for the star-shaped and wounded spiral motions. The curves have the identical evolution subject to two initial conditions. Application of our proposed CCD scheme to predict mean curvature driven motion of curves is therefore justified.

4.3. Prediction of motion of curves driven by mean curvature flow

The linear part of the R.H.S. of Eq. (9) exhibits that the solution ϕ shall be smeared from a higher ϕ value to a lower ϕ value all over the space until the Laplacian of ϕ approaches zero. The source terms in R.H.S. of Eq. (9) including Laplacian and nonlinear terms are always nonzero since ϕ is the distance function. As a result, the motion of curve is always activated until it is shrunk to a point. Three cases of different initial curves are investigated in this section, namely the dumbbell-like, star-like and dumbbell-star-like curves. They are denoted as the cases 1, 2 and 3, respectively. We will also show how the applied reinitialization procedure affects the motion of curve.

Fig. 3 shows the predicted motion driven by mean curvature for case 1. It can be observed that each point on the curve begins to shrink in different speeds along the curve. Curves with a higher curvature have a higher speed. The shape of the curve at $t = 0.0$ is gradually evolved to an ellipse at $t = 2.0$, and it can be expected that the curve will be finally evolved to a circle since it has the lowest surface energy in its physical meaning. From Eq. (9), it is revealed that the motion of the curve is attributed to the effects of linear and nonlinear terms. It is worthy to know which source term is the dominant one in the time evolution and has a stronger effect on the curve.

Figs. 6a and 6b show the relation among the curvature κ, linear source term $\nabla^2\phi$ and nonlinear source term $N(\phi)$ for the solution at $t = 1.0$ with and without reinitialization. The relation is given along the curve $\Gamma(s)$ by introducing a parameter s. $N(\phi)$ is found to have a very small magnitude in comparison with that of $\nabla^2\phi$, implying that the evolution of the mean curvature driven curve is dominated by the diffusion process. Another way to understand why Eq. (9) can be regarded as the linear diffusion equation with reinitialization procedure is that $\nabla\phi = 1$ is satisfied when applying reinitialization procedure in every computational step. According

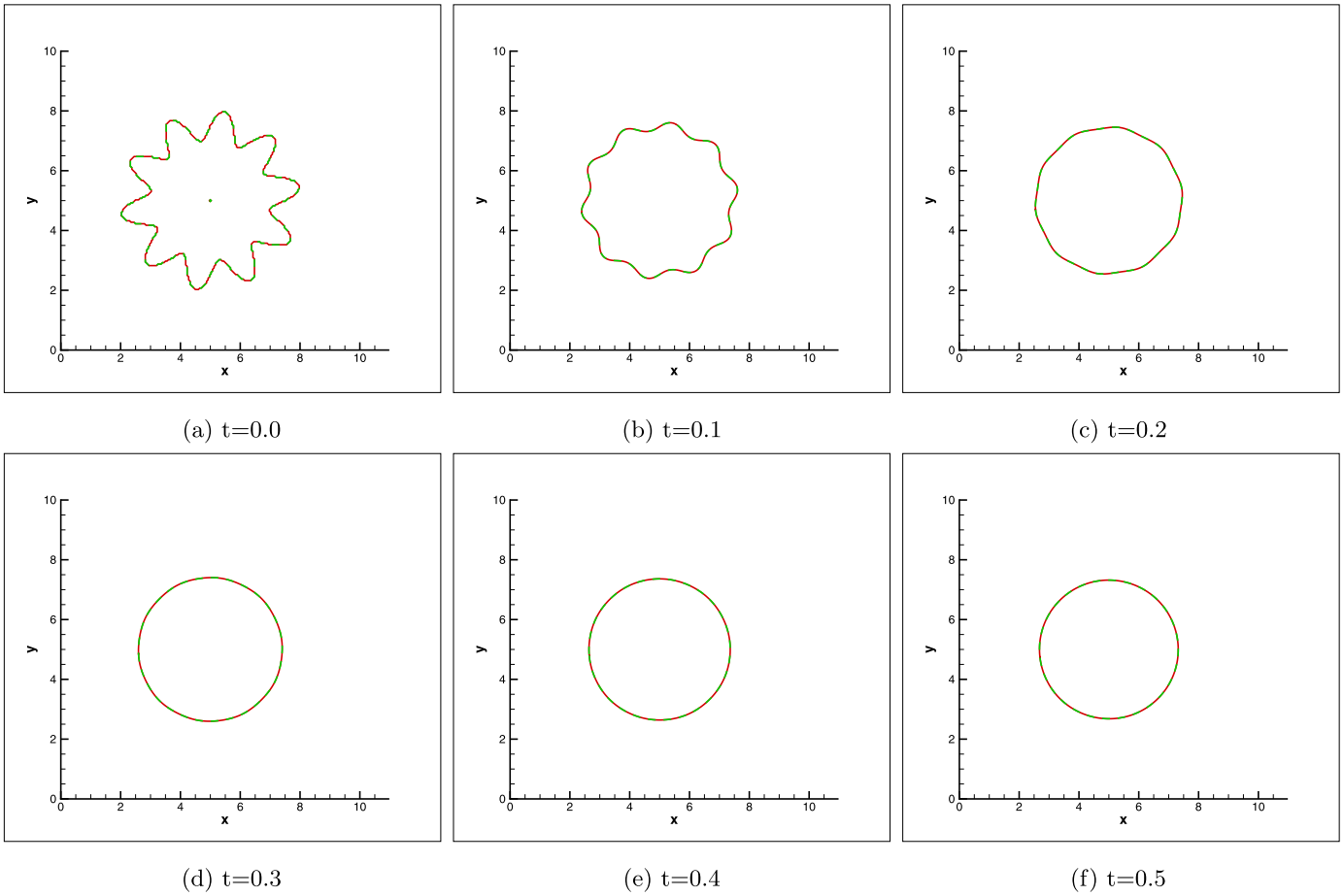

Fig. 4. Case 2. Computation is carried out in 200×200 grids in a 10 by 10 domain, with the mesh size of $h = \Delta x = \Delta y = 0.05$ and the time step of $\Delta t = 0.01 \times h$. Red line denotes the solution obtained with reinitialization procedure while green dashed line denotes the solution obtained without reinitialization procedure. (For interpretation of the references to colour in this figure legend, the reader is referred to the web version of this article.)

to the definition of $N(\phi)$ in Eq. (10), it should be zero under a perfect reinitialization by which the derivative of a constant is zero. Since discretization error will be introduced more or less in the reinitialization step , the value of $N(\phi)$ shall not be exactly equal to zero.

Reinitialization plays an important role in the motion of curve as it is shown in Fig. 6b, since this procedure redistributes $\nabla^2\phi$ and $N(\phi)$ but without affecting the motion of curves as it is shown in Fig. 3. To illustrate how reinitialization affects $\nabla^2\phi$ and $N(\phi)$ in Eq. (9), the following two ratios are defined

$$\omega_L = \frac{|\nabla^2\phi|}{|\nabla^2\phi| + |N(\phi)|}$$
$$\omega_N = \frac{|N(\phi)|}{|\nabla^2\phi| + |N(\phi)|} \tag{33}$$

Fig. 7a shows that the ratio ω_N along the curve **with** reinitialization procedure being made at $t = 1.0$. ω_N is nearly a constant and is close to zero until the curvature approaches zero and becomes negative on $\Gamma(s)$. Also, the maximum of ω_N occurs at $\kappa = 0$. The ratios of the nonlinear terms $N(\phi)$ along the curve are all smaller than 0.05. As a result, Eq. (9) can be regarded as the diffusion dominated equation with the implementation of reinitialization procedure. Fig. 7b shows the evolution of ω_N **without** reinitialization at $t = 1.0$. A very different relation between κ and ω_N is shown. Starting from the value of 0.2, ω_N increases its value while curvature decreases. The maximum also occurs at $\kappa = 0$. Afterwards, ω_N is rapidly decreased to zero while the curvature of curve keeps decreasing. It is worthy to note here that the relation between ω_N and curvature κ depends on the sign of κ in the sense that

$$\frac{\partial^2\omega_N}{\partial\kappa^2} < 0 \quad \text{and} \quad \frac{\partial\omega_N}{\partial\kappa} = 0\Big|_{\kappa=0} \tag{34}$$

Fig. 8a shows that at $t = 2.0$ the linear source term still dominates the nonlinear term with the reinitialization procedure being applied. The ratio $N(\phi)$ is nearly a constant and its value is close to zero along the curve as it is shown in Fig. 9a. Apparently, the solution for the case without performing reinitialization procedure exhibits oscillatory solution, which indicates the deficiency of WENO scheme. Solutions of κ, $\nabla^2\phi$ and $N(\phi)$ are oscillating along the curve, as it can be seen in Fig. 8b, while the solutions in Fig. 8a behave differently. In Fig. 9b, ω_N for the solution obtained at $t = 2.0$ without reinitialization procedure looks similarly to that predicted at $t = 1.0$. Since the curvature along the curve at $t = 2.0$ is positive, ω_N and κ satisfy $\frac{\partial\omega_N}{\partial\kappa} < 0$.

Prediction of a more complex shape of curve helps us to explain the reason of using the combined compact scheme to solve Eq. (9). Fig. 4 shows the motion of the time evolving curve for case 2, which contains a more complicated curvature evolution along the curve. As we mentioned that the motion of the curve is driven by curvature, in physical sense the motion of curve can be considered to be driven by surface tension force. This type of motion has a tendency to reach its minimal surface energy (or minimal surface area), or minimal perimeter in the current two dimensional studies. As it can be seen in Fig. 4, the curve gradually becomes a circle at $t = 0.3$.

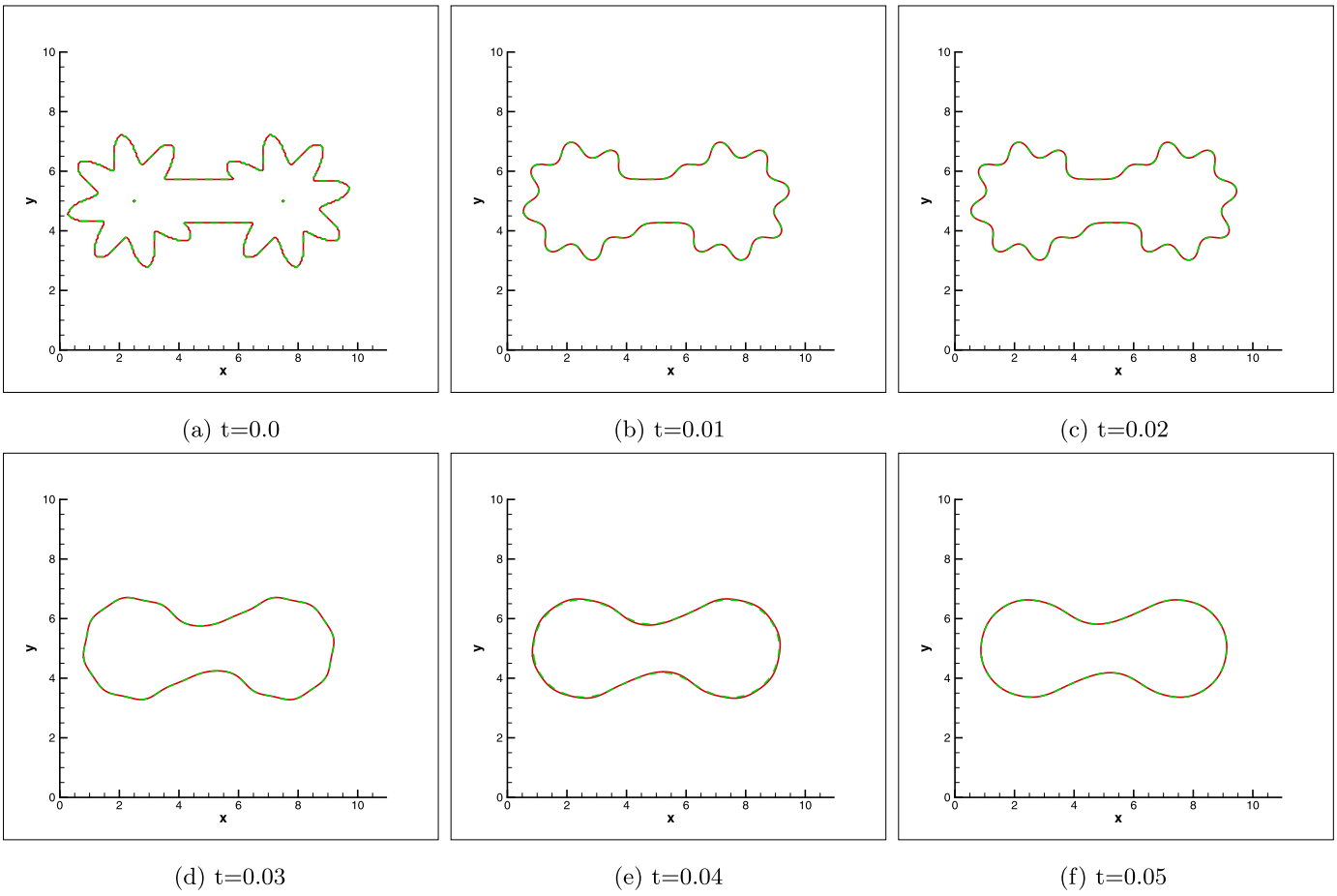

Fig. 5. Case 3. Computation is carried out in 200×200 grids in a 10 by 10 domain, with the mesh size of $h = \Delta x = \Delta y = 0.05$ and the time step of $\Delta t = 0.01 \times h$. Red line denotes the solution obtained with reinitialization procedure while green dashed line denotes the solution obtained without reinitialization procedure. (For interpretation of the references to colour in this figure legend, the reader is referred to the web version of this article.)

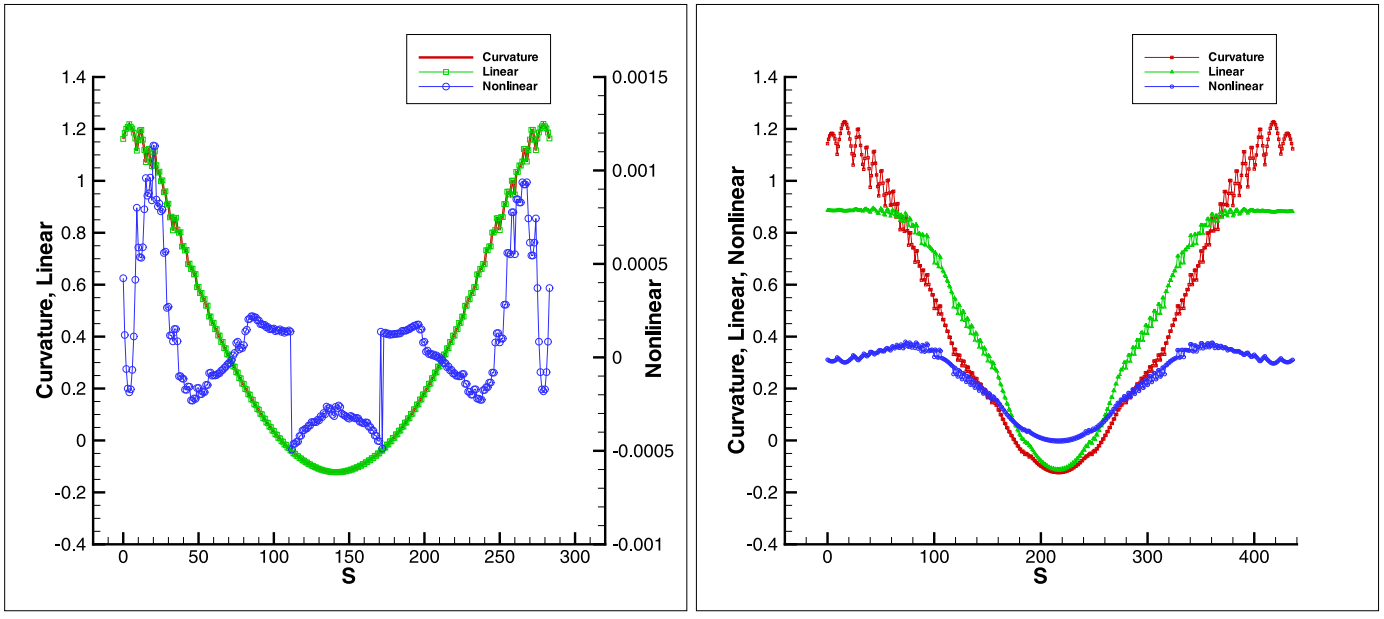

Fig. 6. Plots for indicating the relation among κ, $N(\phi)$ and $\nabla^2\phi$ along the curve $\Gamma(s)$ at $t = 1.0$ for case 1. (a) with reinitialization procedure; (b) without reinitialization procedure.

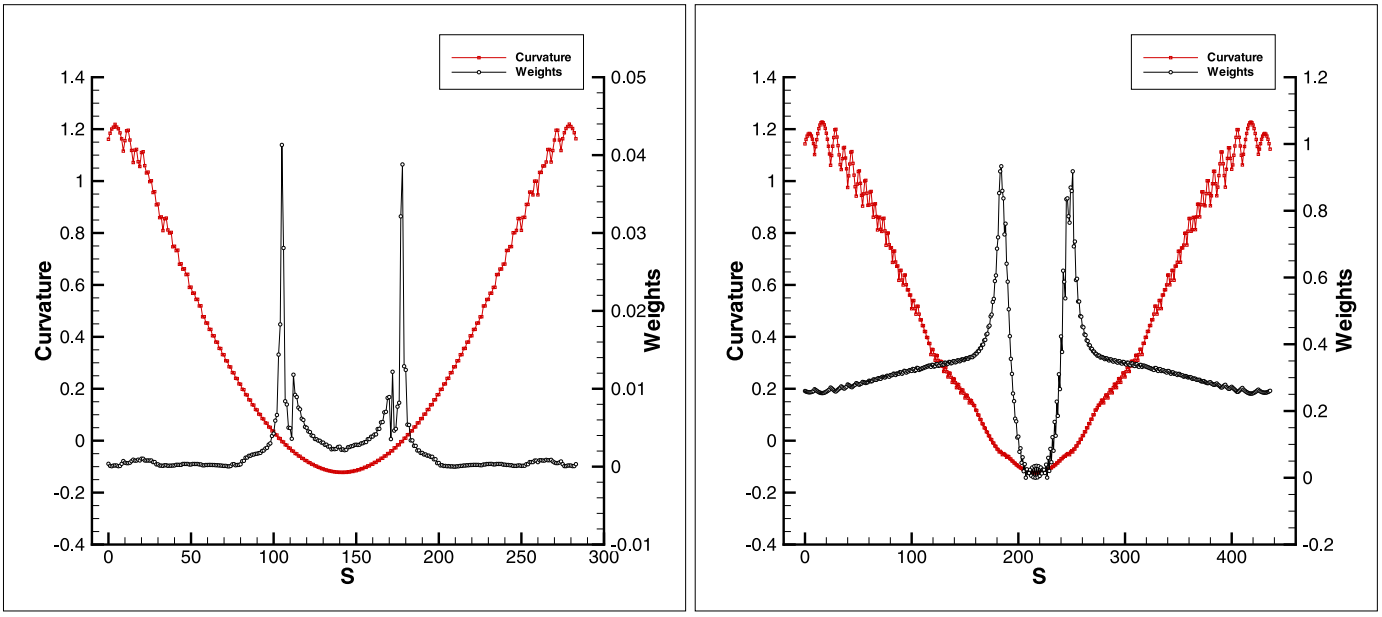

Fig. 7. Plots for ω_N along the curve $\Gamma(s)$ at $t = 1.0$ for case 1. (a) with reinitialization procedure; (b) without reinitialization procedure.

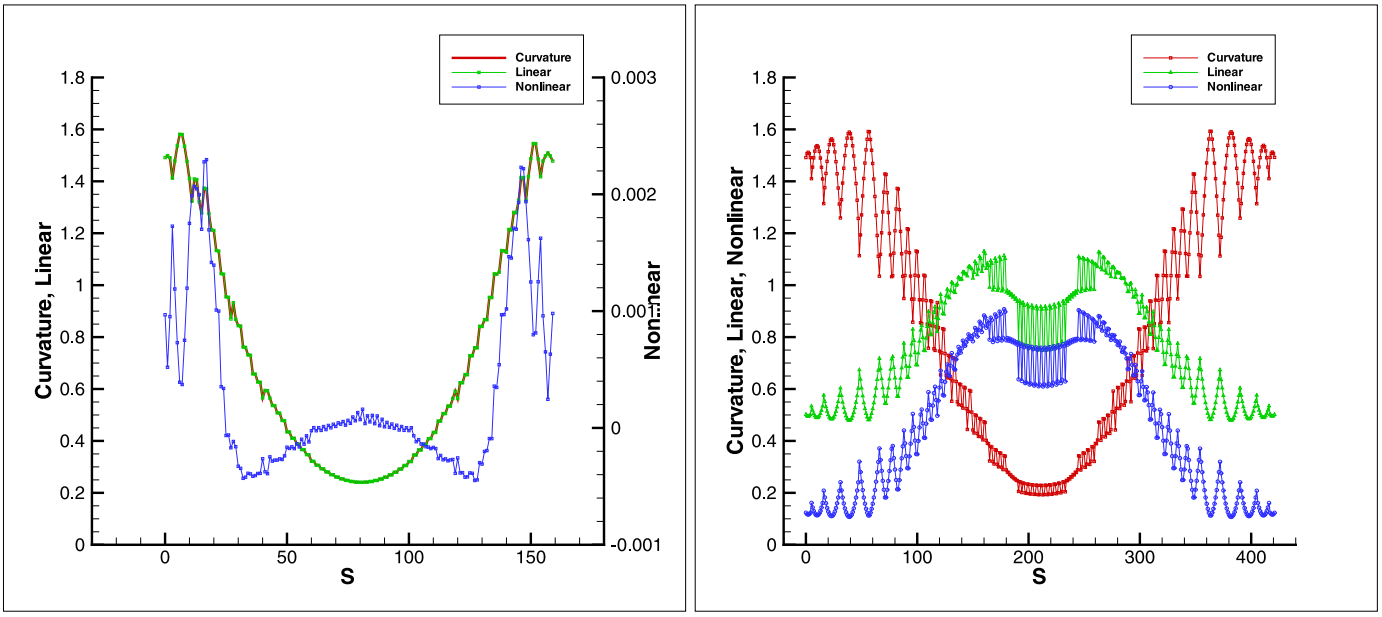

Fig. 8. Plots for indicating the relation among the κ, $N(\phi)$ and $\nabla^2\phi$ along the curve $\Gamma(s)$ at $t = 2.0$ for case 1. (a) with reinitialization procedure; (b) without reinitialization procedure.

The curve with a complicated evolution and a discontinuity in curvature is then considered for showing the capability of applying the CCD scheme to solve Eq. (9). Fig. 5 shows the evolution of the curve for case 3. In this case, a dramatic change of the curvature is seen along the curve. Note that case 3 is nothing but adding a star-like curve to the two sides of the dumbbell-like curve. Minimal perimeter is reached at both sides of the curve in the beginning of motion and, then, to the whole curve. Fig. 10a shows the ratio of nonlinear term $N(\phi)$ for the predicted solution without performing reinitialization in case 3 at $t = 0.05$. The evolution of curve is also dominated by diffusion, due to the application of reinitialization procedure. The maximum of ω_N occurs at $\kappa = 0$, just like that predicted in case 1. Fig. 10b exhibits the evolution of ω_N from the solution without reinitialization and ω_N and κ also satisfy Eq. (34). Fig. 10a and 10b show the solutions with and without reinitialization. Both solutions are oscillatory due to the discontinuous curvature along the curvature. However, while reinitialization procedure is performed, eikonal function $|\nabla\phi| = 1$ is satisfied, and this results in a smoother solution. It's worthwhile to note that the curve continuously evolves even the curve has reached its minimal perimeter. By virtue of Eq. (13), the motion is known to be driven by its local curvature. Since curvature is a positive constant

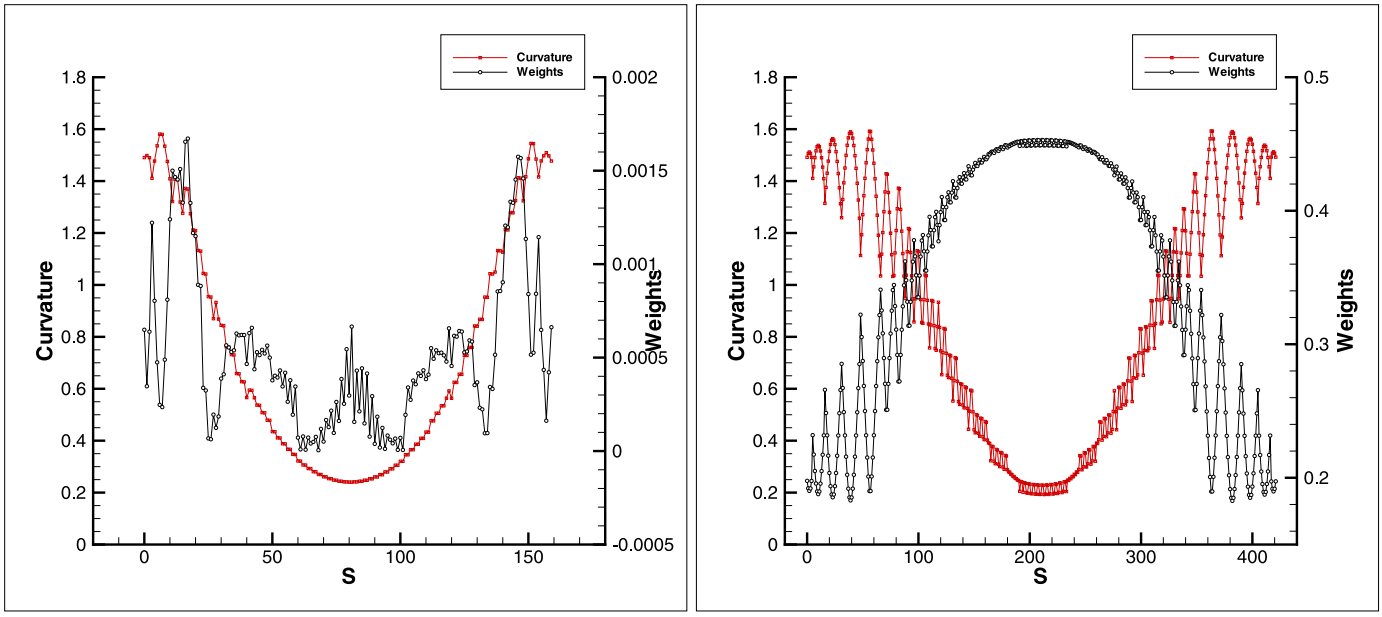

Fig. 9. Plots for ω_N along the curve $\Gamma(s)$ at $t = 2.0$ for case 1. (a) with reinitialization procedure; (b) without reinitialization procedure.

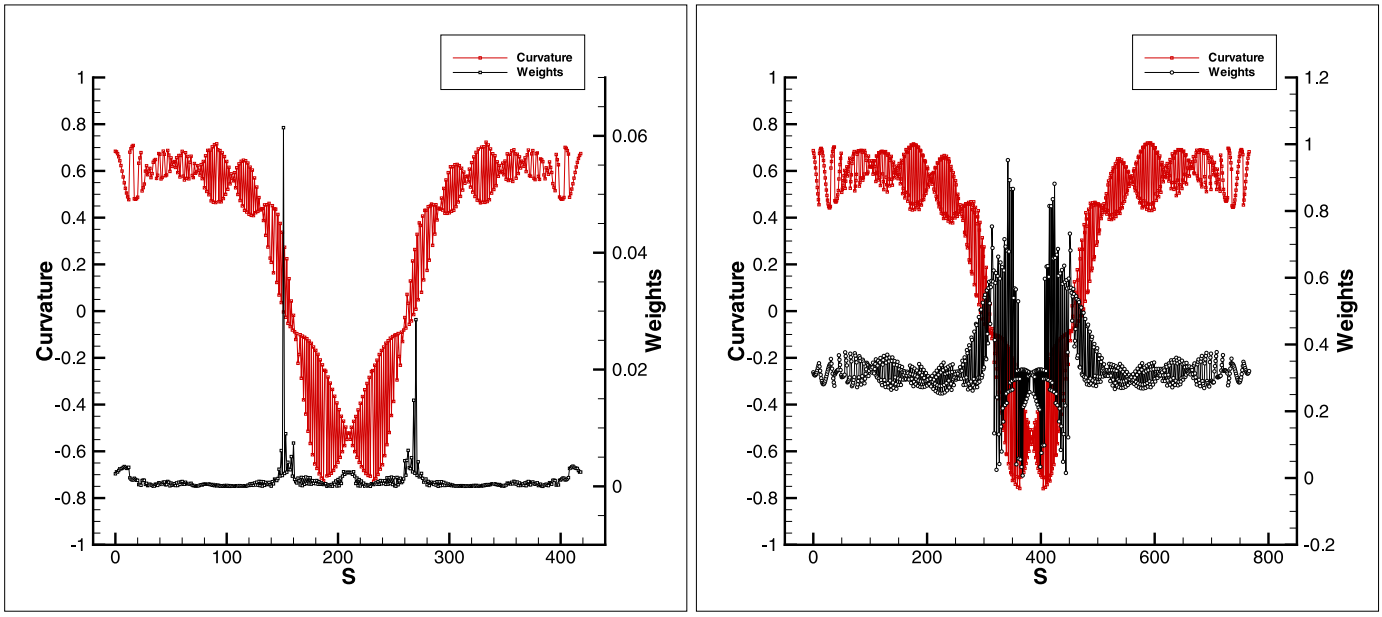

Fig. 10. Plots for ω_N along the curve $\Gamma(s)$ at $t = 0.05$ for case 3. (a) with reinitialization procedure; (b) without reinitialization procedure.

on the perfect circle, the curve keeps shrinking until it becomes a point.

In summary, three mean curvature flows have been investigated by using CCD and TVD-RK3 schemes. All the cases under investigation have shown the tendency to reach their minimal perimeter locally or globally. Reinitialization does not affect the motion of curves, but it can redistribute the ratio of the linear and nonlinear terms on the R.H.S. of Eq. (9). Solutions obtained with reinitialization procedure are strongly affected by the linear source term in Eq. (9). As a result, mean curvature flow can be regarded as being under the control of pure diffusion of distance function ϕ when reinitialization procedure is applied. Solution obtained without reinitialization procedure is oscillatory in comparison with the smooth solution with reinitialization procedure being performed. The ratio of the nonlinear term increases while the curvature decreases in the region with $\kappa > 0$. This ratio reaches its maximum at $\kappa = 0$, and then decreases with the curvature while $\kappa < 0$.

4.4. Comparison of solutions obtained by CCD and second-order centered schemes

In this section, the reason of applying CCD scheme to predict the motion of curves will be explained through several studies in

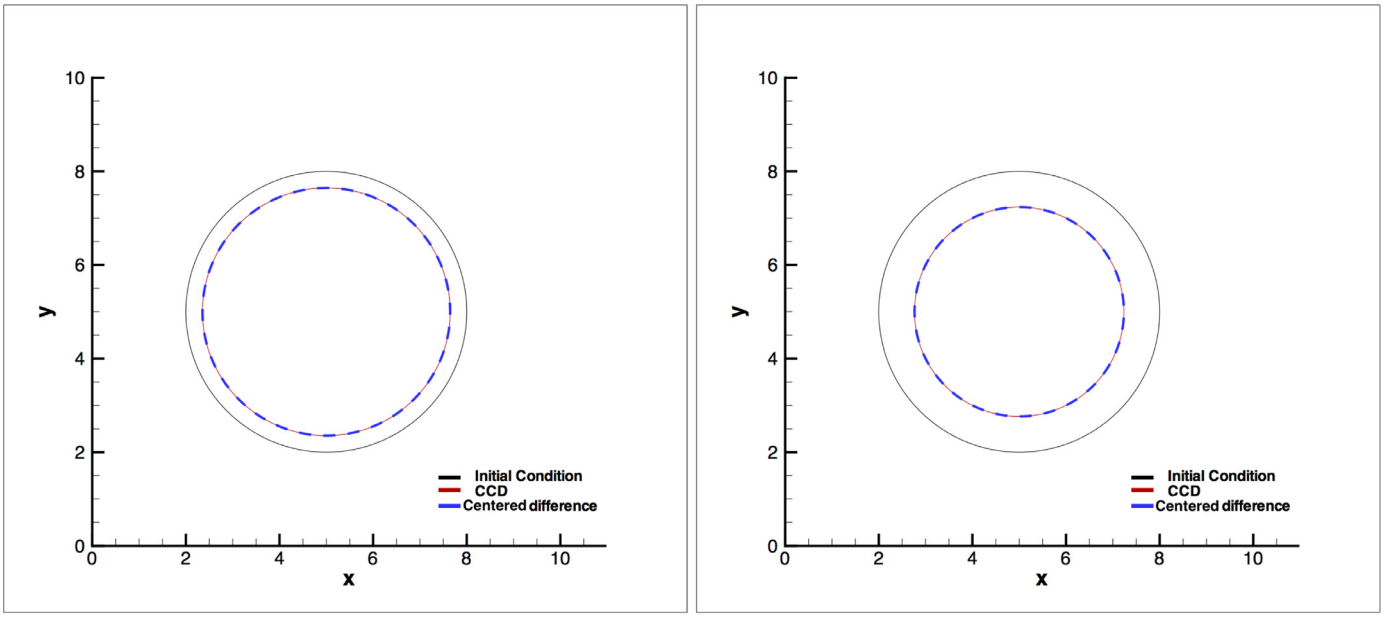

Fig. 11. Task 1. Comparison of the solutions sought at different times by applying the CCD scheme and the second-order centered difference scheme. The computations are carried out with $h = dy = dx = 0.05$ and $dt = 0.01 \times h$. (a) $t = 1.0$; (b) $t = 2.0$.

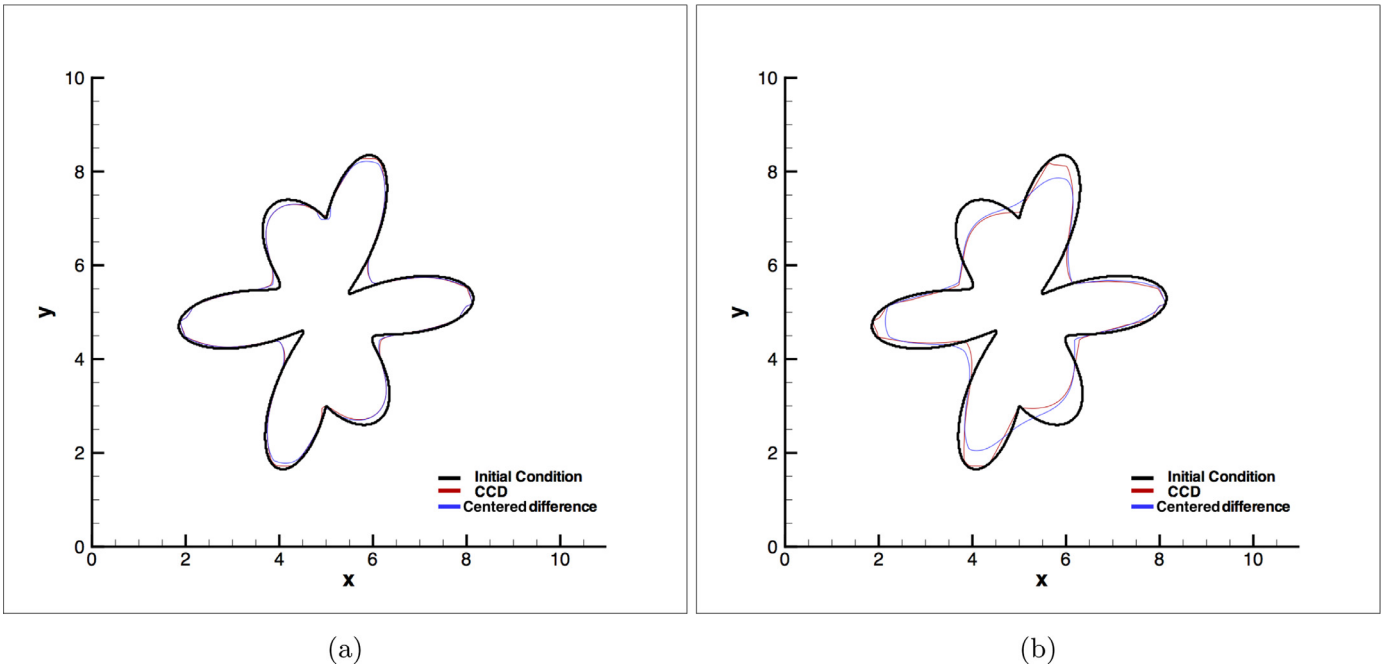

Fig. 12. Task 2. Comparison of the solutions sought at different times by applying the CCD scheme and the second-order centered difference scheme. The computations are carried out with $h = dy = dx = 0.05$ and $dt = 0.01 \times h$. (a) $t = 0.0625$; (b) $t = 0.250$.

this subsection. Initially, the shape of the curve is given as

$$\sqrt{(x-x_0)^2+(y-y_0)^2} = 2.0 + 1.0\cos(\omega_1\theta) + 0.5\sin(\omega_2\theta) \tag{35}$$

where $\theta = \tan^{-1}[(y-y_0)/(x-x_0)]$. The degree of complexity of the curve is determined by the coefficients, ω_1 and ω_2. The larger values of ω_1 and ω_2, the larger change of curvatures along the curve. In a box [10,10], the center of the curve is located at $(x_0, y_0) = (5, 5)$.

4.4.1. Task 1, $(\omega_1, \omega_2) = (0, 0)$

Investigation of this case is to show that either CCD or second-order centered difference scheme is applicable to disctetize the spatial derivatives. Two solutions remain smooth and are identical with each other. In this task, the choice of $\omega_1 = \omega_2 = 0$ results in a circle. As it is shown in Fig. 11, two solutions are identical during the evolution of two curves. Constant curvature is seen along the curve. Both CCD and second-order centered schemes yield accurately simulated evolutions.

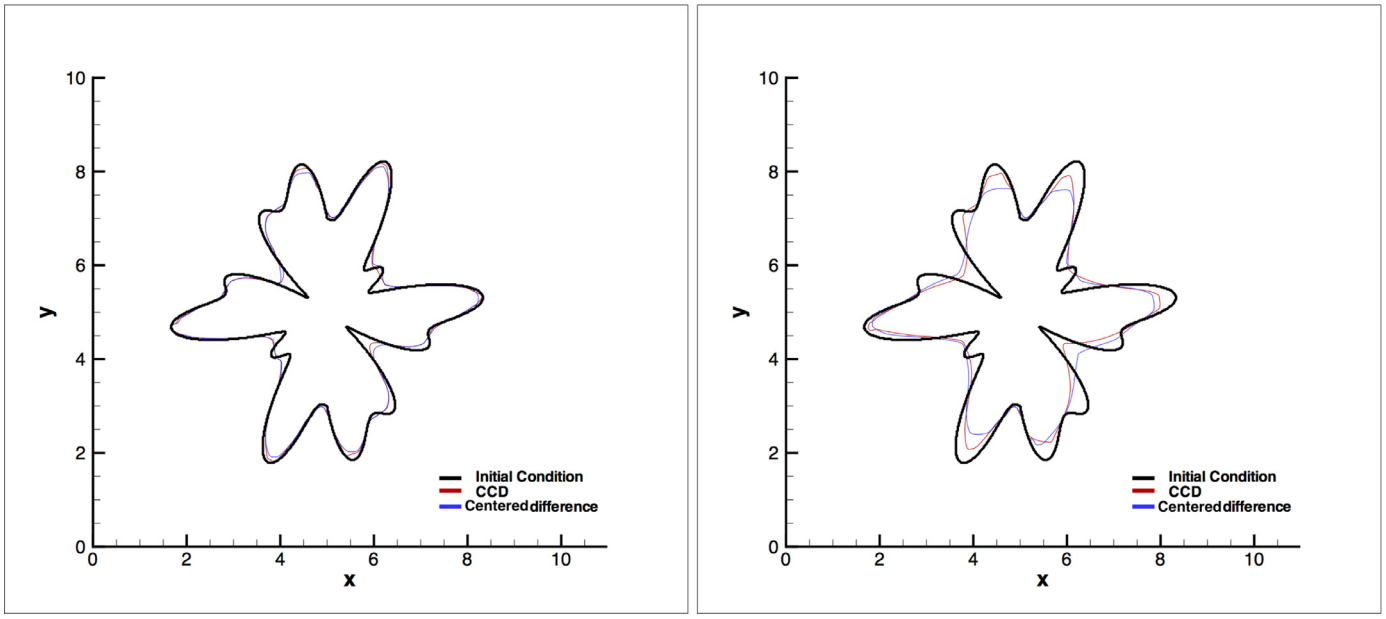

Fig. 13. Task 3. Comparison of the solutions sought at different times by applying the CCD scheme and the second-order centered difference scheme. The computations are carried out with $h = dy = dx = 0.05$ and $dt = 0.01 \times h$. (a) $t = 0.0625$; (b) $t = 0.250$.

4.4.2. Task 2, $(\omega_1, \omega_2) = (5, 6)$

Another task involves variable curvatures by setting $\omega_1 = 5$ and $\omega_2 = 6$ in (35). According to the snap shot of the predicted curve, the solution sought from the second-order centered scheme is more dissipated in the vicinity of the convex and concave parts of the curve. In other words, application of the second-order centered difference scheme yields a smoother solution due to a largely introduced discretization error in the approximation of spatial derivatives. By applying the CCD scheme, one can calculate the curvature term more accurately than that using the second-order centered scheme. As a result, the solution obtained from the CCD scheme is less polluted by the dissipation error introduced to regions with a large curvature, or along the convex and concave parts of the curve.

4.4.3. Task 3, $(\omega_1, \omega_2) = (5, 12)$

Fig. 13 shows the predicted motion of the curve with a more complicated curvature than the curve investigated in task 2. As we mentioned earlier, the solutions obtained from the second-order centered difference scheme are smeared more quickly than CCD scheme does in the sense of introducing more artificial viscosity in the coarse of the simulation of Eq. (9).

In summary, it is advantageous to apply the CCD scheme to capture more accurately the motion of curves with less dissipation error being added to the convex and concave parts of curve. Second-order centered difference scheme also provides a good prediction of the motion of curve in case that the curvature does not change rapidly along the curve. If the shape of curve is too complicated, second-order centered difference scheme is not recommended especially in the very beginning phase of the calculation.

5. Concluding remarks

Within the framework of semi-discretization schemes, an optimal third-order accurate TVD Runge–Kutta temporal scheme for time derivative term and a fifth-order accurate combined compact difference scheme for spatial derivative terms in the level set equation have been developed in a three-point grid stencil. This computationally efficient finite difference scheme has been applied to simulate mean curvature driven motion of curves, subject to different initial curves, with great success. Our main objective of this study is to enlighten how two different mechanisms control the evolution of curve and how they are related to the curvature of the curve under investigation. In the evolution, the surface tension driven curve is subject all the time to the damping effect applied on each point of the curve.

References

[1] Hildebrandt S, Karcher H. Geometric analytic and nonlinear partial differential equations. New York: Springer-Verlag Berlin Heidelberg; 2003. ISBN 3-540-44051-8.
[2] Dierkes U, Hildebrandt S, Sauvigny F. Minimal surface, grundlehren der mathematischen wissenschaften. Berlin Springer-Verlag; 1992.
[3] Smereka P. Semi-implicit level set methods for curvature and surface diffusion motion. J Sci Comput 2003;19:439–56.
[4] Osher S, Fedkiw RP. Level set methods: an overview and some recent results. J Comput Phys 2001;169:463–502.
[5] Sethian JA. Level set methods: evolving interfaces in geometry, fluid mechanics, computer vision, and materials science. Cambridge University Press; 1996.
[6] Sethian JA, Smereka P. Level set methods for fluid interface. Ann Rev Fluid Mech 2003;35:341–72.
[7] Chopp DL. Motion by intrinsic laplacian of curvature. Interfaces Free Boundary 1999;1:107–23.
[8] Khenner M, Averbuch A, Israeli M, Nathan M. Numerical simulation of grain-boundary grooving by level set method. J Comput Phys 2001;170:764–84.
[9] Tasdizen T, Whitaker R, Burchard P, Osher S. Geometric surface processing via normal maps. UCLA CAM report; 2002. 02–03
[10] Shu CW, Osher S. Efficient implementation of essentially non-oscillatory shock-capturing schemes. J Comput Phys 1968;77:439–61.
[11] Gottlieb S, Shu CW. Total variation diminishing runge-kutta schemes. Math Comput 1998;67:73–85.
[12] Chu PC, Fan C. A three point combined compact difference scheme. J Comput Phys 1998;140:370–99.
[13] Sussman M, Smereka P, Osher S. A level set approach for computing solutions to incompressible two-phase flow. J Comput Phys 1994;114:146–59.
[14] Liu XD, Osher S, Chan T. Weighted essential non-oscillatory schemes. J Comput Phys 1994;115:200–12.
[15] Jiang GS, Shu CW. Efficient implementation of weighted ENO schemes. J Comput Phys 1996;126:202–28.
[16] Cheng LT, Tsai R. Redistancing by flow of time dependent eikonal equation. J Comput Phys 2008;227:4002–17.

[17] Shu CW. High order ENO and WENO schemes for computational fluid dynamics. In: Barth TJ, Deconinck H, editors. High-order methods for computational physics. Lecture notes in computational science and engineering, vol. 9. Springer; 1999. p. 439–582.
[18] Osher S, Sethian JA. Fronts propagating with curvature-dependent speed: algorithms based on Hamilton-Jacobian formulations. J Comput Phys 1988;79:12–49.
[19] Hartmann D, Meinke M, Schroder W. Differential equation based constrained reinitialization for level set methods. J Comput Phys 2008;227:6821–45.
[20] Russo G, Smereka P. A remark on computing distance functions. J Comput Phys 2000;163:51–67.